10.18323/2782-4039-2025-2-72-4

Mechanical and corrosion anisotropy of magnesium single crystal

Dmitry L. Merson*[1,3], Doctor of Sciences (Physics and Mathematics), Professor,
Director of the Research Institute of Advanced Technologies
Sergey Ya. Betsofen[2,4], Doctor of Sciences (Engineering), Professor, professor of Chair
"Technologies and Systems for Computer-Aided Design of Metallurgical Processes"
Evgeny D. Merson[1,5], PhD (Physics and Mathematics), senior researcher
of the Research Institute of Advanced Technologies
Vitaly A. Poluyanov[1,6], PhD (Engineering), junior researcher
of the Research Institute of Advanced Technologies
Pavel N. Myagkikh[1,7], PhD (Engineering), junior researcher
of the Research Institute of Advanced Technologies
Aleksey V. Danyuk[1,8], PhD (Physics and Mathematics), senior researcher
of the Research Institute of Advanced Technologies
Vladimir A. Danilov[1,9], PhD (Engineering), junior researcher
of the Research Institute of Advanced Technologies
Ekaterina I. Maksimenko[2], postgraduate student
Aleksandr I. Brilevskiy[1,10], PhD (Engineering), junior researcher
of the Research Institute of Advanced Technologies

[1]*Togliatti State University, Togliatti (Russia)*
[2]*Moscow Aviation Institute, Moscow (Russia)*

***E-mail:** d.merson@tltsu.ru

[3]ORCID: https://orcid.org/0000-0001-5006-4115
[4]ORCID: https://orcid.org/0000-0003-0931-2839
[5]ORCID: https://orcid.org/0000-0002-7063-088X
[6]ORCID: https://orcid.org/0000-0002-0570-2584
[7]ORCID: https://orcid.org/0000-0002-7530-9518
[8]ORCID: https://orcid.org/0000-0002-7352-9947
[9]ORCID: https://orcid.org/0000-0001-5099-6940
[10]ORCID: https://orcid.org/0000-0002-5780-6094

Received 13.12.2024 *Revised 19.03.2025* *Accepted 14.04.2025*

Abstract: Magnesium and its alloys are promising materials for medical use due to their ability to dissolve safely in the human body. However, the rate of dissolution of bioresorbable implants should be in a narrow enough range. The difficulty in ensuring this condition is that the corrosion process in magnesium alloys is influenced by many factors, including natural (single-crystal) and technological (production scheme) anisotropy. By carrying out technological operations on thermomechanical treatment, it is possible to control the process of formation of the semi-finished product texture and to create artificially a preferred orientation of crystallites in the structure of magnesium alloys and thus control their corrosion resistance. This requires precise knowledge of the relationship between corrosion processes and certain crystallographic directions, which can be most reliably obtained in experiments on single crystals. In this work, mechanical (compression and tension) and corrosion tests were carried out for the first time on the same magnesium single crystal on samples with different crystallographic orientations. The Kearns coefficients calculated from the X-ray diffraction patterns of the single crystal specimen faces by the inverse pole figure method were used as a quantitative criterion of the natural texture. The specimens were subjected to compression tests in the $< 0001 >$, $< 1\bar{1}00 >$ and $< 11\bar{2}0 >$ directions, and to tension tests in the $< 0001 >$ direction. The specimen surfaces with orientations close to the (0001), $(10\bar{1}0)$, $(2\bar{1}\bar{1}0)$, and $(10\bar{1}1)$ crystallographic planes were subjected to corrosion testing. It was found that the Young's modulus and the Kearns coefficient for the basal and pyramidal faces were 48.6 GPa and 0.81; 45.3 GPa and 0.04, respectively. The shape of the stress curves depended significantly on the sample orientation and was determined by the degree of involvement of various mechanisms in the overall plastic deformation process. The rate of corrosion in a physiological aqueous solution of 0.9 % NaCl on a 72-h basis for the (0001), $(10\bar{1}0)$, $(2\bar{1}\bar{1}0)$, and $(10\bar{1}0)$ surfaces was 0.51, 0.76, 0.71 and 0.98 mm/year, respectively. In this case, the $(2\bar{1}\bar{1}0)$ plane experienced only uniform corrosion, the (0001) plane experienced uniform corrosion with minor localised corrosion; the most intense localised corrosion is observed in the $(10\bar{1}0)$ direction, and the maximum intensity of the combination of localised and uniform corrosion is in the $<10\bar{1}1>$ direction.

Keywords: magnesium single crystal; crystallographic directions; anisotropy; Kearns coefficient; mechanical diagrams; corrosion rate.

Acknowledgements: The work was supported by the Russian Science Foundation, project No. 23-19-00636 (https://rscf.ru/project/23-19-00636/).

For citation: Merson D.L., Betsofen S.Ya., Merson E.D., Poluyanov V.A., Myagkikh P.N., Danyuk A.V., Danilov V.A., Maksimenko E.I., Brilevskiy A.I. Mechanical and corrosion anisotropy of magnesium single crystal. *Frontier Materials & Technologies*, 2025, no. 2, pp. 39–52. 10.18323/2782-4039-2025-2-72-4.

INTRODUCTION

The study and design of magnesium alloys is one of the up-to-date areas of modern materials science, since these materials have a set of unique properties, such as the best strength-to-weight ratio and excellent biocompatibility: pure magnesium is absorbed by a living organism with a minimal risk of negative effects [1; 2]. One of the main problems when using magnesium alloys is their low corrosion resistance that has a galvanic nature [3], and often manifests itself in the form of localised corrosion [4], which can be significantly affected by the composition and structural state of the material. It is well known that Mg and its alloys are characterised by significant anisotropy of mechanical properties due to the features of the deformation mechanism and the formation of an intense basal texture in sheet semi-finished products, and an intense prismatic texture in extruded rods [5; 6].

Understanding the nature of the corrosion anisotropy of magnesium and its alloys will help determine the structural and textural factors affecting the rate and uniformity of the corrosion process. Consequently, knowledge of the target structure and texture of the material will allow choosing the method of deformation treatment of the product (semi-finished product), or its surface at the final stage of manufacture to produce a material with high-quality and guaranteed parameters of the corrosion process. The rate and uniformity of corrosion are understood as quality parameters. The use of magnesium alloys as a material for the manufacture of temporary implants capable of self-absorbing after fulfilling their intended service is currently a relevant up-to-date sector at the junction of materials science and medicine. Therefore, understanding the corrosion process of magnesium materials and managing it is extremely important for the creation of bioresorbable medical materials with an accurately predictable service life. The same applies to structural magnesium alloys used to manufacture power elements in the aviation and automotive industries. Such elements are made in most cases from semi-finished products manufactured by various methods of metal pressure processing (extrusion, rolling, methods of severe plastic deformation, etc.), the consequence of which is the inevitable formation of a corresponding texture in the processed metal, the parameters of which can significantly affect the corrosion processes. In other words, the corrosion resistance of products made from a material with identical chemical and even phase composition may differ essentially depending on the production technology. Therefore, understanding the cause-and-effect relationships between the structural and textural parameters of magnesium alloys and corrosion processes is of great scientific and applied importance.

However, studies of the effect of texture on the corrosion properties of magnesium alloys have not received due attention in the literature for a long time. Only after 2010, a pronounced trend towards conducting such studies emerged [7–10]. In the work [7], the microstructure, texture, mechanical properties and corrosion behaviour of extruded Mg–4Zn alloy were studied. Samples with an orientation close to the basis showed lower corrosion rates compared to the orientation of samples with a predominance of prismatic planes. In [8–10], similar results were obtained for the AZ31 alloy. Corrosion anisotropy has been experimentally found both in pure magnesium [11] and in deformable magnesium alloys. For example, work [12] presents the results of corrosion rate assessment in various technological directions after rolling of AZ80 alloy, and shows that the corrosion rate determined by the mass method can differ by 1.7 times in the normal direction (ND) and in the extrusion direction (ED). Such a difference in corrosion rate is quite significant and must be taken into account, especially when creating bioresorbable structures for medical purposes.

It is generally accepted that corrosion anisotropy associated with crystallographic orientation is determined by the surface atomic-binding energy and the packing density of atoms [13]. Obviously, such a binding can be most correctly revealed during corrosion tests of single crystals. Surprisingly few such studies have been performed on single crystals of metals with a hexagonal close-packed (hcp) lattice, especially on magnesium. In the earliest work [14], it was found for magnesium single crystals that in a chlorine-containing environment, the (0001) basal plane exhibits the lowest corrosion resistance, and the corrosion itself has a filiform, i. e. it spreads in a direction rather than chaotically, and this direction is determined largely by the crystallographic orientation. In [15], where the corrosion process was studied on single-crystal magnesium planes with the widest possible range of directions, the (0001) orientation, on the contrary, showed the highest corrosion resistance. It should be noted that in most known cases it is the (0001) basal plane that exhibits maximum resistance to corrosion, for example, such a conclusion was made in [11] using the example of a study of a polycrystal of pure magnesium with a large grain.

Along with corrosion anisotropy, magnesium and its alloys are even more characterised by mechanical anisotropy, which is expressed in sharply different mechanical behaviour depending on the crystallographic direction of loading. It is worth noting that there are only a few more experimental studies of mechanical anisotropy performed on magnesium single crystals than studies that cover corrosion anisotropy. The earliest ones include studies [16; 17], in which magnesium single crystals were tested for compression in various directions and only the initial region including the transition from the elastic to the plastic stage was studied. Perhaps the most interesting study of the mechanical behaviour of magnesium single crystals also under compression,

but up to failure, was conducted in [18]. This work convincingly demonstrated the fundamental difference in the compression diagrams of single crystals tested in different crystallographic directions, which is explained by the different combination of twinning and slip deformation mechanisms under starting stresses.

Note that we are not aware of any work in which mechanical and corrosion anisotropy would be simultaneously studied on samples of the same magnesium single crystal.

The purpose of the study is to evaluate and compare corrosion and mechanical anisotropy performed on the same magnesium single crystal.

METHODS

A magnesium single crystal with 99.98 % purity and dimensions of 30×19×62 mm was produced at the Magnesium Technology Innovation Center, School of Materials Science and Engineering, Seoul National University, using the Bridgman method.

The following samples were prepared from the magnesium single crystal by the electrical discharge machining (EDM) using a Sodick AG400L LN2W electric spark wire-cutting machine: (1) in the form of parallelepipeds with dimensions of 6.5×6.0×5.5 mm for compression testing and (2) in the form of specimens of a dog bone shape with cross-section dimensions of 4.0×3.0 mm and a gauge part length of 9.0 mm for tensile testing. Due to the small size of the original single crystal, tensile specimens were prepared for only one <10$\bar{1}$1> orientation. The drawing and orientation of the tensile specimens are shown in Fig. 1.

The orientation of the samples was determined using a SIGMA scanning electron microscope (Zeiss) equipped with an electron backscatter diffraction detector (EBSD).

The mechanical tests of magnesium samples were carried out at room temperature using a miniature Kammrath & Weiss testing machine with a strain rate of $0.83 \cdot 10^{-3}$ s^{-1} for both compression and tension.

The texture was studied by the X-ray diffraction method using a SHIMADZU XRD-6000 vertical 2Θ-Θ X-ray diffractometer (Japan) in monochromatic copper radiation. The texture was estimated by the method of inverse pole figures (IPF) obtained from X-ray patterns for the faces of the specimens parallel to the basal planes, using normalisation that takes into account the uneven distribution of reflections on the projection sphere using the A_i coefficients. The values of the pole densities P_i for reflections $i=hkl$ were determined by the relation

$$P_i = \frac{I_i / R_i}{\sum_{i=1}^{n} A_i \left(I_i / R_i \right)}, \quad (1)$$

where A_i is the ratio of the surface area of the stereographic triangle around the normal $(i=hkl)$ limited by large circles dividing in half the angular distances between adjacent normals;

n is the number of experimental reflections (n=17);

I_i and R_i are the intensities of reflections $i=hkl$ of textured and textureless specimens.

As a quantitative criterion of texture, the Kearns coefficients (f-factors) were used, which are usually used as

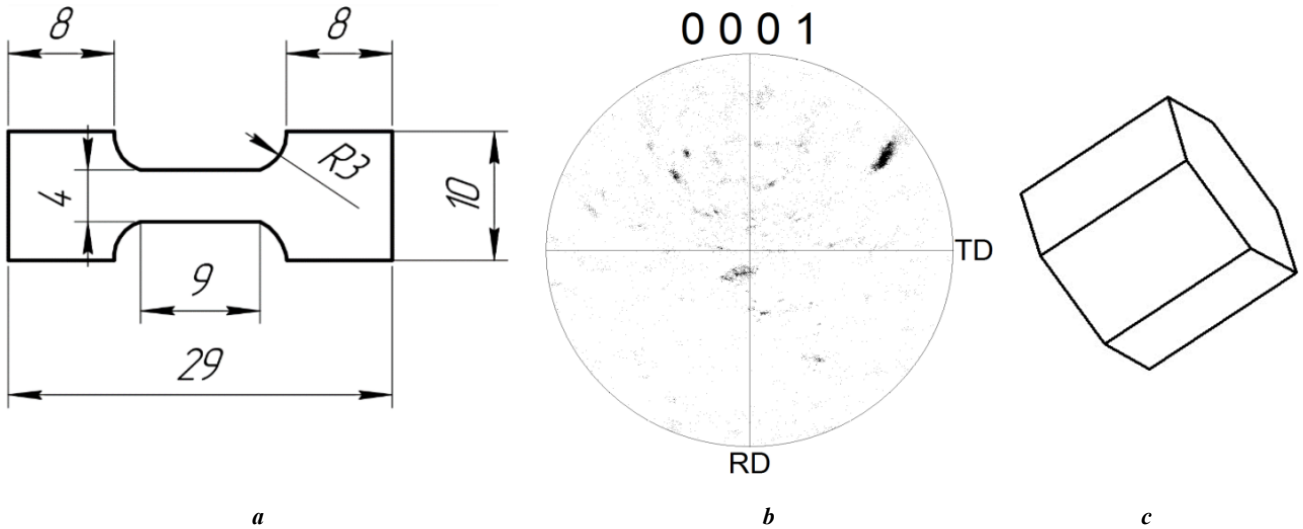

Fig. 1. *Drawing of single crystal magnesium tensile specimens (**a**), steriographic projection of the <0001> crystallographic direction (**b**) and lattice orientation against the longitudinal axis (**c**)*

Рис. 1. *Чертеж образцов монокристалла магния на растяжение (**a**), стериографическая проекция кристаллографического направления <0001> (**b**) и ориентация решетки по отношению к продольной оси (**c**)*

texture parameters in relation to Zr and Ti [19] alloys. The Kearns coefficients are estimated from the inverse pole figures for the *X* direction of the specimen:

$$f_x = \sum_{i=1}^{n} Ai\, P_i^x f_i, \qquad (2)$$

where $i=hkl$;
γ_i is the angle between the normal to (*hkl*) and the *c*-axis of the hcp magnesium lattice.

The Kearns coefficient (f_i) varies from zero for any directions in the basal plane to unity for the normal to the basal plane (*c*-axis).

Moreover, the data on texture obtained as an inverse pole figure were used to calculate the Young's modulus in the direction for which this pole figure was obtained, taking into account the reference values of single-crystal moduli of the material. Young's moduli for hcp of crystals depend only on the γ angle with the *c*-axis:

$$E\gamma = \left[S_{11} - \cos^2\gamma\left(2S_{11} - 2S_{13} - S_{44}\right) + \right.$$
$$\left. + \cos^4\gamma\left(S_{11} + S_{33} - 2S_{13} - S_{44}\right)\right]^{-1}. \qquad (3)$$

Then the value of Young's modulus in an arbitrary *x* direction can be determined from the relation

$$E_x = \sum_{i=1}^{n} P_i^x A_i E_i. \qquad (4)$$

The values of single-crystal compliance moduli for Mg are given in Table 1 [20].

To study the relationship between corrosion processes and the crystallographic directions of the magnesium crystal lattice, parallelepiped-shaped samples were cut from a single crystal using EDM cutting. The orientation of certain faces of the parallelepipeds was close to the orientations of the (0001), $(10\bar{1}0)$, $(2\bar{1}\bar{1}0)$, and $(10\bar{1}1)$ crystallographic planes, respectively, for samples numbered 1, 2, 3, and 4. Before testing, the working faces of the samples were polished sequentially using alcohol diamond suspensions with particle sizes of 3, 1, and 0.25 μm, and then subjected to ion polishing in a flow of ionised argon using a Hitachi IM4000 Plus machine (Japan). After that, using EBSD method, the crystallographic orientation of the working surface of the samples was precisely determined (shown in the inverse pole figure in Fig. 2).

Corrosion tests of samples 1–4 of the magnesium single crystal were carried out using an original corrosion unit [21] for 72 h. During the test, only the area of the sample working surface limited by a sealing ring with an internal diameter of 4 mm was in contact with the corrosion solution. A physiological aqueous solution of 0.9 % NaCl was used as the corrosion medium. Maintaining the temperature in the cell at the level of 37±0.2 °C, as well as mixing the liquid, was ensured by circulating the corrosion solution using a peristaltic pump and a glass heat exchanger immersed in a thermostat tank with distilled water.

After testing, corrosion products were removed from the sample surface by immersing the sample for 2 min in a standard aqueous solution of 20 % CrO_3 + 1 % $AgNO_3$. Then, the samples were washed with alcohol, dried with compressed air, and the surface of the single-crystal samples damaged by corrosion was examined using a LEXT OLS4000 confocal laser scanning microscope (CLSM) (Olympus, Japan). Imaging was performed at a magnification of 400× with a scanning step along the *Z*-axis of 0.8 μm. A panoramic image of 6×6 frames was built for the entire sample. The size of one frame was 640×640 μm. In order to remove optical noise after imaging, a digital

Table 1. *Values of the ductility moduli of Mg [21]*
Таблица 1. *Значения модулей податливости Mg [21]*

Unit of measurement / direction	S_{11}	S_{12}	S_{13}	S_{33}	S_{44}
10^{-2} GPa^{-1}	2.21	−0.78	−0.49	1.99	6.03

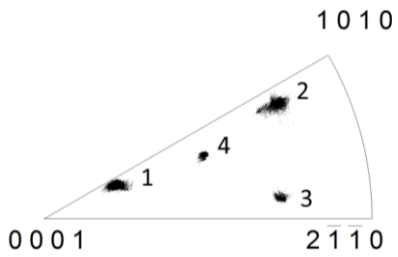

Fig. 2. *Inverse pole figure indicating the crystallographic orientation of the working surface of magnesium single crystal samples 1–4*
Рис. 2. *Обратная полюсная фигура с указанием кристаллографической ориентации рабочей поверхности образцов монокристалла магния 1–4*

pre-measurement filter built into the microscope software was applied to all the obtained images. After filtering, taking the surface of the sample that was not in contact with the corrosive environment as the base reference point, the volume of metal lost in the area of the sample damaged by corrosion was measured. The corrosion rate was determined by formula using CLSM data [22]:

$$P = \frac{87600 \cdot V}{S \cdot t} \text{ (mm/year)}, \quad (5)$$

where V is the volume of lost metal;
S is the area of the sample;
t is the test time.

RESULTS

Texture study

Fig. 3 a, 3 b show X-ray diffraction patterns of a magnesium single crystal indicating that it is indeed a single crystal. Additional confirmation of this is provided by the results of recording rocking curves (Fig. 3 c), according to which the block misorientation value Δα is 0.8 and 1.8°, indicating very low fragmentation of the subgrain structure.

Tables 2 and 3 show the results of texture intensity assessment for the single crystal, which correspond to the X-ray diffraction patterns obtained for the basal and prismatic faces (Fig. 3 a and 3 b), respectively.

The Kearns coefficient for normals to the basal face is 0.81, which is impossible to obtain on polycrystals. The Young's modulus is 48.6 GPa (Table 2), which, according to equation (3), is achieved at angles with the c-axis of 15°. For the lateral prismatic plane $(1\bar{1}00)$ (Fig. 3 b), the Young's modulus is 45.3 GPa, the Kearns coefficient is 0.04, which corresponds to this orientation. The Kearns coefficient is zero for the prismatic plane.

Mechanical tests

Compression test

The compression test of parallelepiped-shaped magnesium single crystal samples was carried out in three mutually perpendicular orientation directions: <0001>, <$1\bar{1}00$>, and <$11\bar{2}0$>. The choice and sequence of the crystallographic direction of external stress application were made in the order from suppression to gradual activation of deformation systems (slip and twinning) with the lowest shear stresses. For the <0001> direction, the easy slip systems in the basal plane are completely blocked, and slip along

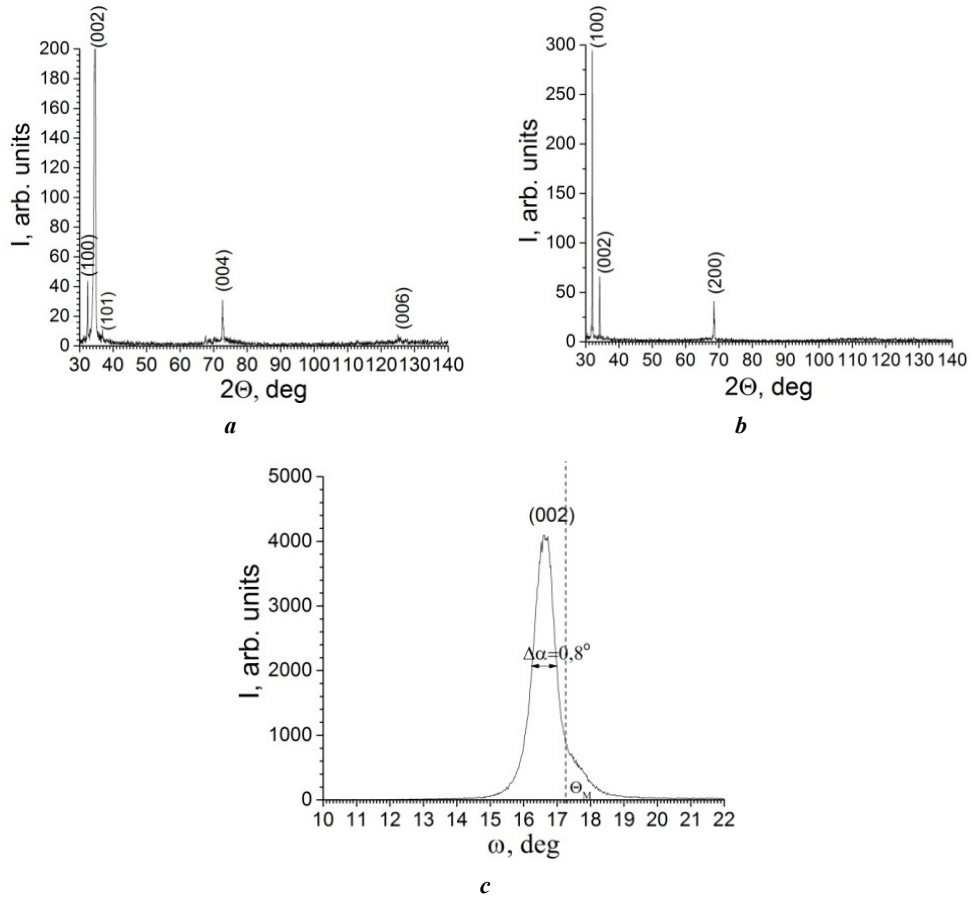

Fig. 3. *X-ray diffraction patterns of faces parallel to:* ***a*** *– basal (0001) and* ***b*** *– prismatic* $(1\bar{1}00)$ *planes;* ***c*** *– ω-scans of a face parallel to the (0001) basal plane*

Рис. 3. *Рентгенограммы граней, параллельных:* ***a*** *– базисной (0001) и* ***b*** *– призматической* $(1\bar{1}00)$ *плоскости;* ***c*** *– ω-сканирования грани, параллельной базисной плоскости (0001)*

Table 2. *Scheme for calculating the Young's modulus and the Kearns coefficient (f-factor) for the basal face*
Таблица 2. *Схема расчета модуля Юнга и коэффициента Кернса (f-фактор) для базисной грани*

hkl	**γ, degree**	E_{hkl}, **GPa**	f	P_{hkl}	A_{hkl}	$P_{hkl}xAxE_{hkl}$	$P_{hkl}xf_{hkl}$
100	90.0	45.2	0.00	1.29	0.044	2.6	0.00
002	0.0	50.3	1.00	48.33	0.016	38.9	0.77
101	61.9	43.3	0.22	0.11	0.044	0.2	0.00
102	43.2	43.4	0.53	0.00	0.059	0.0	0.00
110	90.0	45.2	0.00	0.00	0.027	0.0	0.00
103	32.0	45.0	0.72	0.00	0.048	0.0	0.00
112	58.4	43.1	0.27	0.42	0.039	0.7	0.00
201	75.1	44.5	0.07	0.51	0.058	1.3	0.00
104	25.1	46.4	0.82	0.00	0.042	0.0	0.00
203	51.3	43.0	0.39	0.00	0.050	0.0	0.00
120	90.0	45.2	0.00	0.00	0.051	0.0	0.00
121	78.6	44.8	0.04	0.00	0.120	0.0	0.00
114	39.1	43.8	0.60	0.00	0.096	0.0	0.00
122	68.1	43.8	0.14	0.00	0.103	0.0	0.00
105	20.6	47.4	0.88	0.00	0.062	0.0	0.00
123	58.8	43.1	0.27	1.11	0.104	5.0	0.030
302	70.4	44.1	0.11	0.00	0.039	0.0	0.00
						E_{ND}=48.6 GPa	F_{ND}=0.81

Note. hkℓ is Miller index describing the planes of the crystal lattice;
γ is an angle between the normal to (hkl) and the c-axis of the hpc magnesium lattice;
f is Kearns coefficient;
E_{hkl} is Young's modulus in the hkl direction;
P_{hkl} is pole density of reflections;
A_{hkl} is the ratio of the surface area of a stereographic triangle around the normal (i=hkl) limited by large circles dividing in half the angular distances between adjacent normals;
E_{ND} is Young's modulus in the direction of the normal to the rolling plane;
F_{ND} is Kearns coefficient in the direction of the normal to the rolling plane.

Table 3. *Calculation scheme for Young's modulus and Kearns coefficient (f-factor) for a prismatic face*
Таблица 3. *Схема расчета модуля Юнга и коэффициента Кернса (f-фактор) для призматической грани*

hkl	**γ, degree**	E_{hkl}, **GPa**	f	P_{hkl}	A_{hkl}	$P_{hkl}xAxE_{hkl}$	$P_{hkl}xf_{hkl}$
100	90.0	45.2	0.00	21.71	0.044	43.2	0.00
002	0.0	50.3	1.00	2.48	0.016	2.0	0.04
101	61.9	43.3	0.22	0.04	0.044	0.1	0.00
102	43.2	43.4	0.53	0.00	0.059	0.0	0.00
110	90.0	45.2	0.00	0.00	0.027	0.0	0.00
103	32.0	45.0	0.72	0.00	0.048	0.0	0.00

Continue of table 3

112	58.4	43.1	0.27	0.00	0.039	0.0	0.00
201	75.1	44.5	0.07	0.00	0.058	0.0	0.00
104	25.1	46.4	0.82	0.00	0.042	0.0	0.00
203	51.3	43.0	0.39	0.00	0.050	0.0	0.00
120	90.0	45.2	0.00	0.00	0.051	0.0	0.00
121	78.6	44.8	0.04	0.00	0.120	0.0	0.00
114	39.1	43.8	0.60	0.00	0.096	0.0	0.00
122	68.1	43.8	0.14	0.00	0.103	0.0	0.00
105	20.6	47.4	0.88	0.00	0.062	0.0	0.00
123	58.8	43.1	0.27	0.00	0.104	0.0	0.00
302	70.4	44.1	0.11	0.00	0.039	0.0	0.00
						E_{ND}=45.3 GPa	F_{ND}=0.04

Note. hkℓ is Miller index describing the planes of the crystal lattice;
γ is an angle between the normal to (hkl) and the c-axis of the hpc magnesium lattice;
f is Kearns coefficient;
E_{hkl} is Young's modulus in the hkl direction;
P_{hkl} is pole density of reflections;
A_{hkl} is the ratio of the surface area of a stereographic triangle around the normal (i=hkl) limited by large circles dividing in half the angular distances between adjacent normals;
E_{ND} is Young's modulus in the direction of the normal to the rolling plane;
F_{ND} is Kearns coefficient in the direction of the normal to the rolling plane.

a limited number of pyramidal systems outside the basal plane is greatly hindered. The <$1\bar{1}00$> and <$11\bar{2}0$> configurations are close to each other in the implementation of slip of prismatic and pyramidal planes in the directions lying in the basal plane and twinning of the "stretching" type, but differ in their more favourable arrangement for activation for the <$11\bar{2}0$> direction. Fig. 4 shows three diagrams of compression tests (one for each orientation) in the "Stress (engineering) – Strain (engineering)" coordinates, where the compressive stresses are conventionally given in the positive direction.

Analysis of the diagrams displayed in Fig. 4 shows that, as expected, the orientation of the single crystal to the direction of the applied uniaxial load has a decisive influence on the type of diagrams, or more precisely, on the mechanisms of plastic deformation realised in certain crystallographic directions. This influence has been well studied in [16–18], so here we will only note the following. When testing samples in all three directions, the Schmid factor for basal slip is zero, so deformation can be carried out by twinning or <*c*+*a*> slip.

When testing samples in the <0001> direction, the $\{10\bar{1}2\}$<$10\bar{1}1$> light tensile twinning cannot act, while the maximum possible strain hardening and rapid exhaustion of the possibility of plastic deformation occur. A similar effect for this orientation was observed in [18] and interpreted as <*c*+*a*> slip.

When testing samples in the <$1\bar{1}00$> direction, first there is a stage of deformation with low strain hardening, after which the loading curve rushes sharply upward, and its appearance becomes completely identical to the previous case. This can be easily explained by the action of $\{10\bar{1}2\}$<$10\bar{1}1$> slight tensile twinning, which for this orientation produces a transfer of the orientation of the single crystal to an orientation located 3° from the *c*-axis. In accordance with the magnitude of the shear for this type of twinning, a deformation of ~6 % is required for complete re-twinning of all grains, which is observed for the stage with low strain hardening (Fig. 4). After this, compression occurs in the <0001> direction, respectively, similar to the previous case.

When testing samples in the <$11\bar{2}0$> direction, $\{10\bar{1}2\}$<$10\bar{1}1$> light tensile twinning is also active, but unlike the previous case, the orientation of the twinned single crystal is characterized by a deviation from the *c*-axis by an angle of ~30°. Such an orientation is favourable for basal slip, which for magnesium has a minimum value of the critical shear stress. However, a high level of plasticity is realized stimulating the formation of a texture that coincides with the slip plane for compression, i. e., a basal texture is formed. Therefore, with increasing deformation, the compression axis approaches the *c*-axis, which reduces the Schmid factor for basal slip and, accordingly, increases the flow stress.

The mechanical properties of a single crystal of pure magnesium found during compression testing in different directions are given in Table 4.

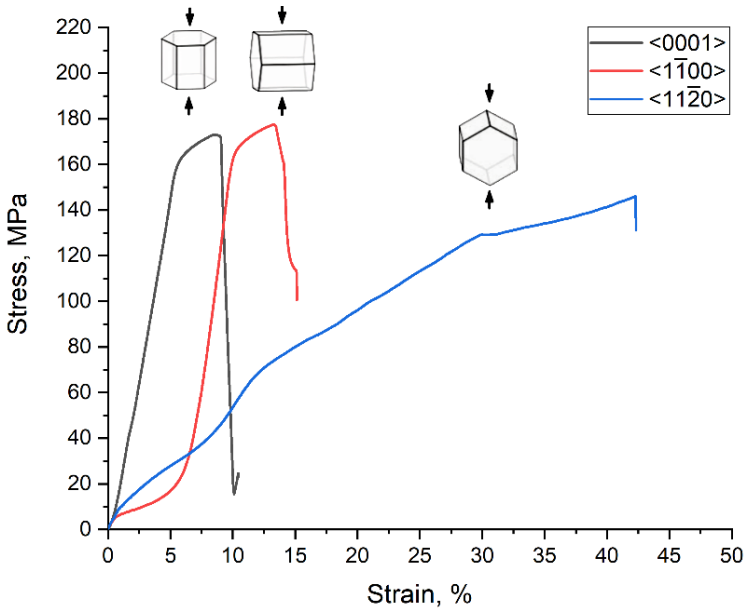

Fig. 4. *Diagrams of compression test of samples of pure magnesium single crystal for three orientations*
Рис. 4. *Диаграммы испытаний образцов монокристалла чистого магния на сжатие для трех ориентаций*

Tension test

The diagram of the tensile test of a magnesium single crystal in the <1$\bar{1}$00> direction is shown in Fig. 5. This direction of loading the single crystal by activation of the deformation systems of the hcp crystal lattice is characterised by high activity of basal slip and “tensile” twinning and, to a lesser extent, slip in prismatic and pyramidal planes. The initial strengthening occurs due to the system of the easiest basal slip for an hcp crystal, which is interrupted by the activation of the “tensile” twinning system at a stress of 32.5 MPa and 2 % deformation, forming a “tooth” in the diagram. The subsequent sharp drop in stress is probably associated with the reorientation of the lattice during twinning to easy slip, i. e. the Schmid factor for basal slip increases, due to which the subsequent deformation occurs at a lower stress. In the range of deformation from 4 to 11 %, a slight strain hardening supported by slight sliding occurs, but after 12 % deformation, a stepwise decrease in strength is observed, which is caused by filling the volume of the sample with intersecting secondary twins with the formation of macrodefects (cracks) at the intersection boundaries. In contrast to compression tests, this direction demonstrates significantly greater plasticity.

Certain standard mechanical properties are given in Table 4.

Corrosion tests

The study of the surface of single crystal samples damaged by corrosion was carried out using CLSM with the reconstruction of surface profiles based on the areas most damaged by corrosion (Fig. 6).

Analysis of the obtained images and profile diagrams indicates, firstly, that the nature of corrosion damage really strongly depends on the crystallographic orientation of the working surface of the single crystal, and secondly, that the (0001) (Fig. 6 a, 6 b) and (2$\bar{1}\bar{1}$0) (Fig. 6 e, 6 f) planes are characterised by uniform corrosion, which is evidenced by

Table 4. *Mechanical properties of magnesium single crystal*
Таблица 4. *Механические характеристики монокристалла магния*

No.	Direction of application of load	Offset yield stress, MPa	Ultimate tensile strength, MPa	Percentage elongation (compression), %
1	<0001> compression	2.55±0.05	170±4	7.5±0.5
2	<1$\bar{1}$00> compression	2.6±0.05	175±5	12.5±0.8
3	<11$\bar{2}$0> compression	2.65±0.05	145±4	42±5
4	<10$\bar{1}$1> tension	8.8±0.2	33±4	34±3

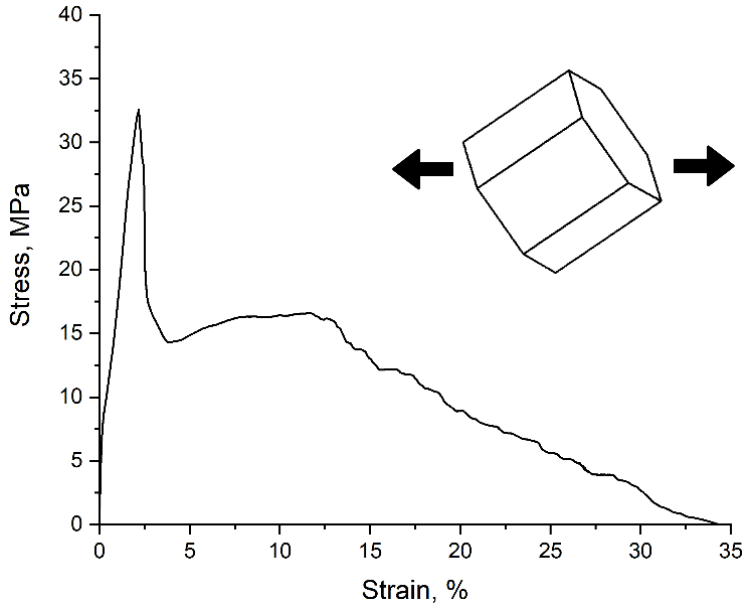

Fig. 5. *Diagram of the test of a pure magnesium single crystal sample for uniaxial tension in the* $<10\bar{1}1>$ *direction*
Рис. 5. *Диаграмма испытания образца монокристалла чистого магния на одноосное растяжение в направлении* $<10\bar{1}1>$

significant depth fluctuations along the entire length of the profile diagrams, while the $(10\bar{1}0)$ (Fig. 6 c, 6 d) and $(10\bar{1}1)$ (Fig. 6 g, 6 h) planes, on the contrary, are characterised by localised corrosion with a pit depth of up to 30 μm with minimal damage to the surface between the pits.

According to confocal microscopy data, the corrosion rate based on 72-hour tests was 0.51±0.04, 0.76±0.08, 0.71±0.07, and 0.98±0.10 mm/year for (0001), $(10\bar{1}0)$, $(2\bar{1}\bar{1}0)$, and $(10\bar{1}1)$ planes, respectively.

DISCUSSION

According to the obtained results (Table 2), the Young's modulus for the basal plane is 48.6 GPa, which is achieved at angles with the *c*-axis of 15°, which is slightly greater than the Young's modulus for the lateral prismatic plane $(1\bar{1}00)$ – 45.3 GPa.

When testing samples in the <0001> direction, the maximum possible strain hardening occurs, which is associated with the action of <c+a> slip. Compression in the $<1\bar{1}00>$ direction is characterised by low strain hardening at the initial stage as a result of the action of slight tensile $\{10\bar{1}2\}<10\bar{1}1>$ twinning, which for this orientation transfers the single crystal orientation of all grains into an orientation spaced away from the c-axis by 3°. This requires a deformation of ~6 %, which is observed experimentally. After this, compression occurs in the <0001> direction. Under compression in $<11\bar{2}0>$, slight tensile $\{10\bar{1}2\}<10\bar{1}1>$ twinning is also active, but the orientation of the twinned single crystal is characterised by a deviation from the c-axis by an angle of ~30°, and such an orientation is favourable for basal slip, which provides high plasticity. With increasing deformation, the compression axis approaches the *c*-axis, which reduces the Schmid factor for basal slip and, accordingly, increases the flow stress.

The corrosion process on the surface of magnesium single crystals can be conditionally divided into two components: uniform and localised. The first involves complete dissolution of the surface layer to a certain depth, and the second is the formation of local pits. It is illustrated by the profile diagrams of the corroded surface of differently oriented surfaces of a magnesium single crystal, shown in Fig. 6. Since part of the working surface of the sample was not in contact with the corrosive environment, it was taken as the zero corrosion level (indicated by a dotted line in Fig. 6 b, 6 d, 6 f, 6 h). The dashed line in Fig. 6 b, 6 d, 6 f, 6 h conventionally denotes the maximum depth of uniform corrosion. From Fig. 6, it follows that the minimum depth h_{un} (rate) of uniform corrosion corresponds to the (0001) plane (~6.5 μm, Fig. 6 b), for all the others, it has close values: ~10, 12.5 and 11.5 μm for the $(10\bar{1}0)$, $(2\bar{1}\bar{1}0)$, and $(10\bar{1}1)$ planes, respectively (Fig. 6 d, 6 f, 6 h). In this case, the maximum pit depth h_{loc} took values of 25, 35, 10, and 22 μm for the (0001), $(10\bar{1}0)$, $(2\bar{1}\bar{1}0)$, and $(10\bar{1}1)$ planes, respectively. According to these results, it becomes obvious that in a magnesium single crystal, the $(10\bar{1}0)$ plane has the greatest tendency to pitting (localised) corrosion (Fig. 6 d), and the $(2\bar{1}\bar{1}0)$ plane has the least tendency (Fig. 6 f). A theoretical explanation for this phenomenon has yet to be found.

Based on the above, the previously given values of corrosion rates of 0.51±0.04, 0.76±0.08, 0.71±0.07, and 0.98±0.10 mm/year for the working (0001), $(10\bar{1}0)$, $(2\bar{1}\bar{1}0)$, and $(10\bar{1}1)$ surfaces, respectively, are the result of superposition of uniform and local corrosion rates.

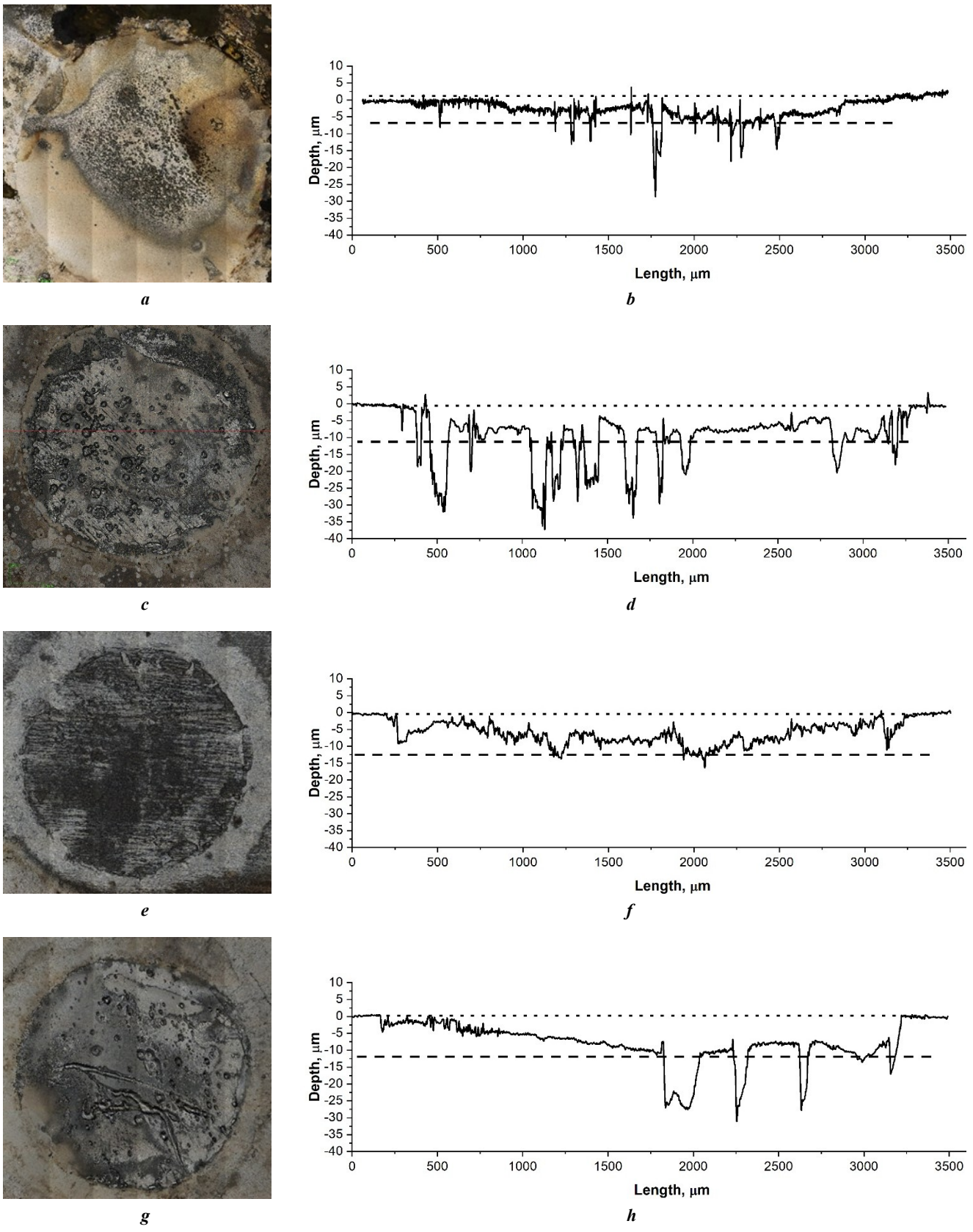

Fig. 6. *Image of corroded surface (**a**, **c**, **e**, **g**) and corresponding profile diagrams (**b**, **d**, **f**, **h**) for working* (0001) *(**a**, **b**),* $(10\bar{1}0)$ *(**c**, **d**),* $(2\bar{1}\bar{1}0)$ *(**e**, **f**), and* $(10\bar{1}1)$ *(**g**, **h**) surfaces according to CLSM data. Dotted line – zero level; dashed line – maximum level of uniform corrosion*

Рис. 6. *Изображение прокорродированной поверхности (**a**, **c**, **e**, **g**) и соответствующие им профилограммы (**b**, **d**, **f**, **h**) для рабочих поверхностей* (0001) *(**a**, **b**),* $(10\bar{1}0)$ *(**c**, **d**),* $(2\bar{1}\bar{1}0)$ *(**e**, **f**) и* $(10\bar{1}1)$ *(**g**, **h**) по данным КЛСМ. Мелкий пунктир – нулевой уровень; средний пунктир – максимальный уровень равномерной коррозии*

It should be noted that, according to the obtained data, the (0001) plane has the lowest average corrosion rate, which is in good agreement with the results of most works by other researchers [11; 15]. At the same time, a detailed analysis of the surface relief shows that the low value of the average corrosion rate of this plane is primarily caused by the low rate of uniform corrosion, while the depth of local corrosion damage in this plane is higher than, for example, in the $(2\bar{1}\bar{1}0)$ and $(10\bar{1}1)$ planes. Thus, at a significantly lower average corrosion rate, the (0001) plane has a rather high tendency to local corrosion compared to other crystallographic planes. It should be considered when designing the microstructure and crystallographic texture of semi-finished and finished products made of magnesium alloys that are planned to be used in contact with aggressive environments. Local corrosion is one of the most dangerous forms of degradation of metallic materials in an aggressive environment, since it can lead to a rapid local decrease in the cross-section of a part and even the occurrence of through damage in thin-walled products. Moreover, corrosion pits formed as a result of the development of this type of corrosion can serve as crack nuclei in stress corrosion cracking. At the same time, until now, corrosion studies on magnesium single crystals have provided data only on the integral assessment of the corrosion rate, which, as shown in this paper, do not always provide a sufficiently complete view of the corrosion resistance of a particular crystallographic plane.

CONCLUSIONS

1. The anisotropy of the elastic properties of a magnesium single crystal is insignificant: Young's moduli for the basal and pyramidal directions are 48.6 and 45.3 GPa, respectively, i. e. they differ by less than 7 %. At the same time, the Kearns coefficient, which is a quantitative criterion of texture, is 20 times higher for the basal plane (0.81) than for the pyramidal plane (0.04).

2. The strong anisotropy of the mechanical properties of a pure magnesium single crystal is caused by the structure of the hcp crystal lattice and a complex combination of the work of crystalline deformation systems of slip and twinning, which differ in configuration. Pure single-crystal magnesium demonstrates a wide range of mechanical parameters: yield strength by 3.5 times, ultimate strength by 5 times, and plasticity by 5.6 times with variations in the direction of application of load to a pure magnesium single crystal.

3. The corrosion rate in an aqueous solution of 0.9 % NaCl on a 72-h basis for the (0001), $(10\bar{1}0)$, $(2\bar{1}\bar{1}0)$, and $(10\bar{1}1)$ surfaces of magnesium single crystals was 0.51±0.04, 0.76±0.08, 0.71±0.07, and 0.98±0.10 mm/year, respectively. At the same time, the $(2\bar{1}\bar{1}0)$ plane experiences only uniform corrosion, and the (0001) plane experiences uniform corrosion with minor localised corrosion; localised corrosion is most intense in the $<10\bar{1}0>$ direction, and the maximum intensity of the combination of localised and uniform corrosion is in the $<10\bar{1}1>$ direction.

REFERENCES

1. Aljihmani L., Alic L., Boudjemline Y., Hijazi Z.M., Mansoor B., Serpedin E., Qaraqe K. Magnesium-Based Bioresorbable Stent Materials: Review of Reviews. *Journal of Bio- and Tribo-Corrosion*, 2019, vol. 5, article number 26. DOI: 10.1007/s40735-019-0216-x.
2. Gu Xue-Nan, Zheng Yu-Feng. A review on magnesium alloys as bio-degradable materials. *Frontiers of Materials Science in China*, 2010, vol. 4, no. 2, pp. 111–115. DOI: 10.1007/s11706-010-0024-1.
3. Song Guangling, Atrens A. Understanding Magnesium Corrosion – A Framework for Improved Alloy Performance. *Advanced Engineering Materials*, 2003, vol. 5, no. 12, pp. 837–858. DOI: 10.1002/adem.200310405.
4. Schmutz P., Guillaumin V., Lillard R.S., Lillard J.A., Frankel G.S. Influence of Dichromate Ions on Corrosion Processes on Pure Magnesium. *Journal of the Electrochemical Society*, 2003, vol. 150, no. 4, pp. B99–B110. DOI: 10.1149/1.1554721.
5. Betsofen S.Y., Osintsev O.E., Grushin I.A., Petrov A.A., Speranskii K.A. Influence of alloying elements on the deformation mechanism and the texture of magnesium alloys. *Russian Metallurgy (Metally)*, 2019, vol. 2019, no. 4, pp. 346–360. DOI: 10.1134/S0036029519040049.
6. Betsofen S.Y., Osintsev O.E., Grushin I.A., Petrov A.A., Speranskii K.A. Texture and anisotropy of the mechanical properties of magnesium alloys. *Russian Metallurgy (Metally)*, 2019, vol. 2019, no. 4, pp. 361–373. DOI: 10.1134/S0036029519040050.
7. Sabbaghian M., Mahmudia R., Shin K.S. Effect of texture and twinning mechanical properties and corrosion behavior of an extruded biodegradable Mg–4Zn alloy. *Journal of Magnesium and Alloys*, 2019, vol. 7, no. 4, pp. 707–716. DOI: 10.1016/j.jma.2019.11.001.
8. Song Guang-Ling, Mishra R., Xu Zhen Qing. Crystallographic orientation and electrochemical activity of AZ31 Mg alloy. *Electrochemistry Communications*, 2010, vol. 12, no. 8, pp. 1009–1012. DOI: 10.1016/j.elecom.2010.05.011.
9. Jiang Bin, Xiang Qing, Atrens A., Song Jiangfeng, Pan Fusheng. Influence of crystallographic texture and grain size on the corrosion behaviour of as-extruded Mg alloy AZ31 sheets. *Corrosion Science*, 2017, vol. 126, pp. 374–380. DOI: 10.1016/j.corsci.2017.08.004.
10. Xin Renlong, Li Bo, Li Ling, Liu Qing. Influence of texture on corrosion rate of AZ31 Mg alloy in 3.5 wt.% NaCl. *Materials & Design*, 2011, vol. 32, no. 8-9, pp. 4548–4552. DOI: 10.1016/j.matdes.2011.04.031.
11. Liu Ming, Qiu Dong, Zhao Ming-Chun, Song Guangling, Atrens A. The effect of crystallographic orientation on the active corrosion of pure magnesium. *Scripta Materialia*, 2008, vol. 58, no. 5, pp. 421–424. DOI: 10.1016/j.scriptamat.2007.10.027.
12. Jian Quantong, Ma Xiumin, Zhang Kui, Li Yantao, Li Xinggang, Li Yongjun, Ma Minglong, Hou Baorong. Anisotropy of the crystallographic orientation and corrosion performance of high-strength AZ80 Mg alloy. *Journal of Magnesium and Alloys*, 2015, vol. 3, no. 4, pp. 309–314. DOI: 10.1016/j.jma.2015.11.002.

13. Gross A. *Theoretical Surface Science: A Microscopic Perspective*. Berlin, Springer Publ., 2003. 342 p. DOI: 10.1007/978-3-540-68969-0.
14. McCall C.R., Hill M.A., Lillard R.S. Crystallographic Pitting in Magnesium Single Crystals. *Corrosion Engineering Science and Technology*, 2005, vol. 40, pp. 337–343. DOI: 10.1179/174327805X66326.
15. Shin Kwang Seon, Bian Ming Zhe, Nam Nguyen Dang. Effects of Crystallographic Orientation on Corrosion Behavior of Magnesium Single Crystals. *JOM*, 2012, vol. 64, pp. 664–670. DOI: 10.1007/s11837-012-0334-0.
16. Wonsiewicz B.C., Backofen W.A. *Plasticity of magnesium crystals*. Massachusetts, Massachusetts Institute of Technology Publ., 1967. 57 p.
17. Kelley E.W., Hosford W.F. *Plane-Strain Compression of Magnesium and Magnesium Alloy Crystals*. 1968. 242 p.
18. Molodov K.D., Al-Samman T., Molodov D.A. On the Plasticity and Deformation Mechanisms in Magnesium Crystals. *Metals*, 2023, vol. 13, no. 4, article number 640. DOI: 10.3390/met13040640.
19. Dzunovich D.A., Betsofen S.Ya., Panin P.V. Methodological aspects of the quantitative texture analysis of HCP alloy (Ti, Zr) sheet semiproducts. *Russian Metallurgy (Metally)*, 2017, vol. 2017, no. 10, pp. 813–820. DOI: 10.1134/S0036029517100056.
20. Shalin R.E., Svetlov I.L., Kachanov E.B., Toloraiya V.N., Gavrilin O.S. *Monokristally nikelevykh zharoprochnykh splavov* [Single crystals of nickel heat-resistant alloys]. Moscow, Mashinostroenie Publ., 1997. 336 p. EDN: PIYTZX.
21. Merson E.D., Poluyanov V.A., Myagkikh P.N., Sergeev A.A., Merson D.L. Relationship between the anisotropy of corrosion properties of extruded AZ31 and ZK60 with crystallographic texture and volume distribution of second-phase particles. *Russian Journal of Non-ferrous Metals*, 2024, vol. 65, pp. 1–10. DOI: 10.1134/S1067821224600832.
22. Danilov V.A., Merson D.L. Quantitative estimation of the corrosion rate of metallic materials using confocal laser scanning microscopy. *Letters on Materials*, 2021, vol. 11, no. 3, pp. 291–297. DOI: 10.22226/2410-3535-2021-3-291-297.

СПИСОК ЛИТЕРАТУРЫ

1. Aljihmani L., Alic L., Boudjemline Y., Hijazi Z.M., Mansoor B., Serpedin E., Qaraqe K. Magnesium-Based Bioresorbable Stent Materials: Review of Reviews // Journal of Bio- and Tribo-Corrosion. 2019. Vol. 5. Article number 26. DOI: 10.1007/s40735-019-0216-x.
2. Gu Xue-Nan, Zheng Yu-Feng. A review on magnesium alloys as bio-degradable materials // Frontiers of Materials Science in China. 2010. Vol. 4. № 2. P. 111–115. DOI: 10.1007/s11706-010-0024-1.
3. Song Guangling, Atrens A. Understanding Magnesium Corrosion – A Framework for Improved Alloy Performance // Advanced Engineering Materials. 2003. Vol. 5. № 12. P. 837–858. DOI: 10.1002/adem.200310405.
4. Schmutz P., Guillaumin V., Lillard R.S., Lillard J.A., Frankel G.S. Influence of Dichromate Ions on Corrosion Processes on Pure Magnesium // Journal of the Electrochemical Society. 2003. Vol. 150. № 4. P. B99–B110. DOI: 10.1149/1.1554721.
5. Бецофен С.Я., Осинцев О.Е., Грушин И.А., Петров А.А., Сперанский К.А. Влияние легирующих элементов на механизм деформации и текстуру магниевых сплавов // Деформация и разрушение материалов. 2018. № 8. С. 2–17. DOI: 10.31044/1814-4632-2018-8-2-17.
6. Бецофен С.Я., Осинцев О.Е., Грушин И.А., Петров А.А., Сперанский К.А. Закономерности формирования текстуры и анизотропии механических свойств магниевых сплавов // Деформация и разрушение материалов. 2018. № 9. С. 2–15. DOI: 10.31044/1814-4632-2018-9-2-15.
7. Sabbaghian M., Mahmudia R., Shin K.S. Effect of texture and twinning mechanical properties and corrosion behavior of an extruded biodegradable Mg–4Zn alloy // Journal of Magnesium and Alloys. 2019. Vol. 7. № 4. P. 707–716. DOI: 10.1016/j.jma.2019.11.001.
8. Song Guang-Ling, Mishra R., Xu Zhen Qing. Crystallographic orientation and electrochemical activity of AZ31 Mg alloy // Electrochemistry Communications. 2010. Vol. 12. № 8. P. 1009–1012. DOI: 10.1016/j.elecom.2010.05.011.
9. Jiang Bin, Xiang Qing, Atrens A., Song Jiangfeng, Pan Fusheng. Influence of crystallographic texture and grain size on the corrosion behaviour of as-extruded Mg alloy AZ31 sheets // Corrosion Science. 2017. Vol. 126. P. 374–380. DOI: 10.1016/j.corsci.2017.08.004.
10. Xin Renlong, Li Bo, Li Ling, Liu Qing. Influence of texture on corrosion rate of AZ31 Mg alloy in 3.5 wt.% NaCl // Materials & Design. 2011. Vol. 32. № 8-9. P. 4548–4552. DOI: 10.1016/j.matdes.2011.04.031.
11. Liu Ming, Qiu Dong, Zhao Ming-Chun, Song Guangling, Atrens A. The effect of crystallographic orientation on the active corrosion of pure magnesium // Scripta Materialia. 2008. Vol. 58. № 5. P. 421–424. DOI: 10.1016/j.scriptamat.2007.10.027.
12. Jian Quantong, Ma Xiumin, Zhang Kui, Li Yantao, Li Xinggang, Li Yongjun, Ma Minglong, Hou Baorong. Anisotropy of the crystallographic orientation and corrosion performance of high-strength AZ80 Mg alloy // Journal of Magnesium and Alloys. 2015. Vol. 3. № 4. P. 309–314. DOI: 10.1016/j.jma.2015.11.002.
13. Gross A. Theoretical Surface Science: A Microscopic Perspective. Berlin: Springer, 2003. 342 p. DOI: 10.1007/978-3-540-68969-0.
14. McCall C.R., Hill M.A., Lillard R.S. Crystallographic Pitting in Magnesium Single Crystals // Corrosion Engineering Science and Technology. 2005. Vol. 40. P. 337–343. DOI: 10.1179/174327805X66326.
15. Shin Kwang Seon, Bian Ming Zhe, Nam Nguyen Dang. Effects of Crystallographic Orientation on Corrosion Behavior of Magnesium Single Crystals // JOM. 2012. Vol. 64. P. 664–670. DOI: 10.1007/s11837-012-0334-0.
16. Wonsiewicz B.C., Backofen W.A. Plasticity of magnesium crystals. Massachusetts: Massachusetts Institute of Technology, 1967. 57 p.
17. Kelley E.W., Hosford W.F. Plane-Strain Compression of Magnesium and Magnesium Alloy Crystals. 1968. 242 p.
18. Molodov K.D., Al-Samman T., Molodov D.A. On the Plasticity and Deformation Mechanisms in Magnesium

Crystals // Metals. 2023. Vol. 13. № 4. Article number 640. DOI: 10.3390/met13040640.
19. Дзунович Д.А., Бецофен С.Я., Панин П.В. Методические аспекты количественного текстурного анализа листовых полуфабрикатов из ГПУ-сплавов (Ti, Zr) // Деформация и разрушение материалов. 2016. № 11. С. 8–16. EDN: XBFIED.
20. Шалин Р.Е., Светлов И.Л., Качанов Е.Б., Толораия В.Н., Гаврилин О.С. Монокристаллы никелевых жаропрочных сплавов. М.: Машиностроение, 1997. 336 с. EDN: PIYTZX.
21. Merson E.D., Poluyanov V.A., Myagkikh P.N., Sergeev A.A., Merson D.L. Relationship between the anisotropy of corrosion properties of extruded AZ31 and ZK60 with crystallographic texture and volume distribution of second-phase particles // Russian Journal of Non-ferrous Metals. 2024. Vol. 65. P. 1–10. DOI: 10.1134/S1067821224600832.
22. Данилов В.А., Мерсон Д.Л. Количественная оценка скорости коррозии металлических материалов с помощью конфокальной лазерной сканирующей микроскопии // Письма о материалах. 2021. Т. 11. № 3. С. 291–297. DOI: 10.22226/2410-3535-2021-3-291-297.

Механическая и коррозионная анизотропия монокристалла магния

Мерсон Дмитрий Львович*[1,3], доктор физико-математических наук, профессор, директор НИИ прогрессивных технологий
Бецофен Сергей Яковлевич[2,4], доктор технических наук, профессор, профессор кафедры «Технологии и системы автоматизированного проектирования металлургических процессов»
Мерсон Евгений Дмитриевич[1,5], кандидат физико-математических наук, старший научный сотрудник НИИ прогрессивных технологий
Полуянов Виталий Александрович[1,6], кандидат технических наук, младший научный сотрудник НИИ прогрессивных технологий
Мягких Павел Николаевич[1,7], кандидат технических наук, младший научный сотрудник НИИ прогрессивных технологий
Данюк Алексей Валериевич[1,8], кандидат физико-математических наук, старший научный сотрудник НИИ прогрессивных технологий
Данилов Владимир Алексеевич[1,9], кандидат технических наук, младший научный сотрудник НИИ прогрессивных технологий
Максименко Екатерина Игоревна[2], аспирант
Брилевский Александр Игоревич[1,10], кандидат технических наук, младший научный сотрудник НИИ прогрессивных технологий

[1]*Тольяттинский государственный университет, Тольятти (Россия)*
[2]*Московский авиационный институт, Москва (Россия)*

***E-mail:** d.merson@tltsu.ru

[3]ORCID: https://orcid.org/0000-0001-5006-4115
[4]ORCID: https://orcid.org/0000-0003-0931-2839
[5]ORCID: https://orcid.org/0000-0002-7063-088X
[6]ORCID: https://orcid.org/0000-0002-0570-2584
[7]ORCID: https://orcid.org/0000-0002-7530-9518
[8]ORCID: https://orcid.org/0000-0002-7352-9947
[9]ORCID: https://orcid.org/0000-0001-5099-6940
[10]ORCID: https://orcid.org/0000-0002-5780-6094

Поступила в редакцию 13.12.2024 *Пересмотрена 19.03.2025* *Принята к публикации 14.04.2025*

Аннотация: Магний и его сплавы относятся к перспективным материалам для применения в медицине в связи с их способностью безопасно растворяться в организме человека. Однако скорость растворения биорезорбируемых имплантатов должна находиться в достаточно узком диапазоне. Сложность обеспечения этого условия состоит в том, что на коррозионный процесс в магниевых сплавах оказывают влияние очень многие факторы, в том числе естественная (монокристальная) и технологическая (схема получения) анизотропия. Путем проведения технологических операций по термомеханической обработке можно контролировать процесс формирования текстуры полуфабриката и искусственно создавать преимущественную ориентацию кристаллитов в структуре магниевых сплавов и таким образом управлять их коррозионной стойкостью. Для этого нужны точные знания о связи коррозионных процессов с определенными кристаллографическими направлениями, которые наиболее надежно можно получить в экспериментах на монокристаллах. В настоящей работе впервые на одном и том же монокристалле магния проведены механические (на сжатие и растяжение) и коррозионные испытания на образцах, имеющих различную кристаллографическую ориентацию. В качестве количественного критерия естественной текстуры использовали коэффициенты Кернса, рассчитанные по рентгенограммам граней образцов монокристалла по методу обратных полюсных фигур. Испытания образцов на сжатие проводили в направлениях $< 0001 >$, $< 1\bar{1}00 >$ и $< 11\bar{2}0 >$, а на растяжение – $< 0001 >$. Коррозионному испытанию подвергали поверхности образцов, близкие по ориентации к кристаллографическим плоскостям (0001), $(10\bar{1}0)$, $(2\bar{1}\bar{1}0)$ и $(10\bar{1}1)$. Установлено, что модуль Юнга и коэффициент Кернса для базисной и пирамидальной граней со-

ставляют 48,6 ГПа и 0,81; 45,3 ГПа и 0,04 соответственно. Вид кривых напряжения существенно зависит от ориентации образцов и определяется степенью вовлеченности различных механизмов в общий процесс пластической деформации. Скорость коррозии в физиологическом водном растворе состава 0,9 % NaCl на базе 72 ч для поверхностей (0001), $(10\bar{1}0)$, $(2\bar{1}\bar{1}0)$ и $(10\bar{1}0)$ составила 0,51; 0,76; 0,71 и 0,98 мм/год соответственно, при этом плоскости $(2\bar{1}\bar{1}0)$ присуща только равномерная коррозия, плоскости (0001) – равномерная с незначительной локальной; наиболее интенсивно локальная коррозия идет в направлении $(10\bar{1}0)$, а максимальная интенсивность сочетания локальной и равномерной – в направлении $<10\bar{1}1>$.

Ключевые слова: монокристалл магния; кристаллографические направления; анизотропия; коэффициент Кернса; механические диаграммы; скорость коррозии.

Благодарности: Работа выполнена при поддержке Российского научного фонда, проект № 23-19-00636 (https://rscf.ru/project/23-19-00636/).

Для цитирования: Мерсон Д.Л., Бецофен С.Я., Мерсон Е.Д., Полуянов В.А., Мягких П.Н., Данюк А.В., Данилов В.А., Максименко Е.И., Брилевский А.И. Механическая и коррозионная анизотропия монокристалла магния // Frontier Materials & Technologies. 2025. № 2. С. 39–52. 10.18323/2782-4039-2025-2-72-4.